Partial Internal Wetting of Catalyst Particles with a Distribution of Pore Size

The recent model of partial internal wetting of catalyst particles (Bhatia, 1988) is extended to allow for pore-size distribution, multicomponent diffusion, and nonlinear kinetics for spherical particles exposed to condensible vapor undergoing an exothermic reaction. Profiles of liquid filling of the pores are computed, and the influence on mass transfer and effectiveness factor is determined. Under certain circumstances, the effectiveness factor has a maximum with respect to the mole fraction of condensible component suggesting an optimum vapor-phase composition. As the bulk vapor approaches saturation the effectiveness factor and particle temperature can drop sharply because of precipitious increase in liquid filling. However, a significant fraction of the pore space is still dry in contradiction to prior models assuming complete internal wetting of catalyst particles. The new model is more realistic than earlier attempts and lays the framework for proper representation of the physical phenomena involved.

S.K. Bhatia
Department of Chemical Engineering
Indian Institute of Technology
Bombay 400 076, India

Introduction

One of the major challenges in the modeling of catalytic trickle-bed reactors is the adequate representation of the effects of partial wetting (both internal and external) of the catalyst particles. Because partial internal wetting can arise even under externally dry conditions (Sedriks and Kenney, 1973; Satterfield and Ozel, 1973; Hanika et al., 1976; Kim and Kim, 1981a), it is generally important to suitably model this effect even in studies of partial external wetting. Lacking such a model, most investigations of partial external wetting (Ramachandran and Smith, 1979; Mills and Dudrkovic, 1980, 1982; Herskowitz, 1981a,b; Yentekakis and Vayenas, 1987; Hu and Ho, 1987; Harold, 1988; Tan, 1988) have considered only completely internally wetted particles. Further progress in the subject, therefore, depends to a large extent on the development of adequate models of partial internal wetting.

While some studies exist (Kim and Kim 1981a,b; Sakornwimon and Sylvester, 1982; Drobyshevich et al., 1983; Bhatia, 1988) of the effect of partial internal wetting, all, except for Bhatia, have considered only thermal and diffusional effects ignoring the vapor-liquid thermodynamics pertinent to such situations. Under conditions of partial internal wetting, it is clear that vapor-liquid equilibria and capillary condensation thermodynamics must also play a role, as recognized by Kim and Kim (1981a), and must be incorporated in the mathematical modeling. The recent work of Bhatia (1988) considers these aspects in addition to the attendant transport effects and represents a step in this direction. In that work, the interplay of capillary condensation phenomena with thermal and diffusional effects on externally dry catalyst particles showed that steady states can exist, in which micropores in an inner core or an outer shell are liquid filled while the remainder of the particle is vapor filled. Under certain conditions, even two such steady states were found although one of them was shown to be unstable.

The previous paper, Bhatia (1988), considered the case of a catalyst particle that comprises uniformly-sized micropores and macropores, and assumed first-order kinetics. In this paper, the case of a particle with an arbitrary bimodal pore-size distribution is analyzed allowing for nonlinearity in the reaction kinetics. The model for such a situation is developed and numerically solved to study the effect of kinetics, dispersion in pore-size distribution, mole fraction of condensible component and Thiele modulus on steady-state behavior and effectiveness factor.

Model Development

We consider the irreversible reaction

$$aA + bB \rightarrow cC \tag{1}$$

occurring in a spherical catalyst particle surrounded by a vapor phase comprising a mixture of A and B. Components A and C are assumed to be condensible while B is not. This system may

be representative of hydrogenation processes in trickle-bed reactors with B being hydrogen. Although both liquid and vapor phases exist in trickle beds, there are always vapor-locked regions due to maldistribution, and this model therefore applies directly to particles in such regions. Even partial external wetting may be represented by assuming that some particles are surrounded by liquid and the remainder by vapor. We consider here only those particles surrounded by the vapor. Even in such particles, capillary condensation will occur in pores smaller than a critical size at any interior radial location causing a reduction in the pore space available for vapor-phase transport and, hence, in the effectiveness factor. We model the above situation under the following assumptions:

1. Boundary layer concentration differences are negligible and mass transfer is controlled by intraparticle diffusion.
2. Heat transfer is controlled by the external boundary layer resistance, and intrapartical temperature gradients are negligible.
3. Micropore effectiveness factor is unity everywhere in both the liquid and vapor phases.
4. Intraparticle transport is dominated by vapor phase diffusion, and radial liquid-phase transport rates are negligible.
5. Reaction rate is controlled by surface reaction and is the same in liquid-filled pores as in the surrounding vapor-filled pores.

All of the above assumptions have been discussed in detail and justified in the prior work (Bhatia, 1988). Assumption 5 considers adsorption as well as the local vapor and liquid phases to be at equilibrium, so that concentrations and chemical potentials of the adsorbed species in the liquid-filled pores are the same as those in the surrounding vapor-filled pores since micropore effectiveness is assumed unity everywhere. This results in equality of the local surface reaction rates in liquid- and vapor-filled pores. This conclusion has also been arrived at earlier, by Sedriks and Kenney (1973), who discussed the subject thoroughly, as well as by Satterfield and Ozel (1973), and more recently by Smith and Satterfield (1986). It is also experimentally verified by the results of Satterfield and Way (1972).

The mathematical formulation of the problem, based on the above assumptions, is as follows.

Mass transfer

For spherical particles, the steady-state conservation equation for species i takes the form

$$\frac{1}{R^2}\frac{d}{dR}(R^2 N_i) = \hat{R}_i \qquad i = 1, 2, 3 \tag{2}$$

where $i = 1$ for A, 2 for B and 3 for C. Following Feng and Stewart (1973), we obtain the flux N_i of species i in the vapor phase by the integration of the pore fluxes over the pore volume:

$$N_i = \frac{1}{\tau}\int_{r_c}^{\infty} N_i(r) f(r)\, dr \tag{3}$$

where τ is a tortuosity factor, $f(r)$ is the pore volume distribution, and r_c is the radius of the smallest pore open to vapor-phase transport at any radial position R in the pellet. Thus, pores in the size range $0 \le r \le r_c$ are liquid-filled due to capillary condensation and unavailable for vapor-phase transport. Equation 3, while derived from the work of Feng and Stewart for a random pore structure, also holds for a structure involving nonoverlapping microporous grains surrounded by macropores, provided the tortuosity factor is the same for macropore diffusion and for diffusion in the grains (Leung and Haynes, 1984).

To relate the pore flux $N_i(r)$ to the local concentration gradient, we use the dusty-gas model equations which, for negligible viscous flow, reduce to the modified Stefan-Maswell form (Kehoe and Aris, 1973; Hite and Jackson, 1977; Jackson, 1977)

$$N_i(r) = -D_{im}(r)\, C_T \frac{dy_i}{dR} \tag{4}$$

where D_{im} is a mixture diffusivity, satisfying

$$\frac{1}{D_{im}} = \sum_{j \ne i}\frac{1}{D_{ij}}\left[y_j - \frac{N_j(r)}{N_i(r)} y_i\right] + \frac{1}{D_{k,i}(r)} \tag{5}$$

and the steady-state flux ratio $N_j(r)/N_i(r)$ is the ratio of the corresponding stoichiometric coefficients. Recognizing that the mole fractions y_i must sum to unity, we utilize only the first two of the differential equations in Eq. 2 and obtain the dimensionless representation

$$\frac{1}{\eta^2}\frac{d}{d\eta}\left(\eta^2 D^*_{eA}\frac{dy_A}{d\eta}\right) = \phi^2 y^o_A \theta \hat{R}^*_A \tag{6}$$

$$\frac{1}{\eta^2}\frac{d}{d\eta}\left(\eta^2 D^*_{eB}\frac{dy_B}{d\eta}\right) = \frac{b}{a}\phi^2 y^o_A \theta \hat{R}^*_A \tag{7}$$

$$y_C = 1 - y_A - y_B \tag{8}$$

$$D^*_{eA}(\eta) = \frac{1}{\epsilon}\int_{\rho_c(\eta)}^{\infty} D^*_{Am}(\rho) f(\rho)\, d\rho \tag{9}$$

$$D^*_{eB}(\eta) = \frac{1}{\epsilon}\int_{\rho_c(\eta)}^{\infty} D^*_{Bm}(\rho) f(\rho)\, d\rho \tag{10}$$

$$D^*_{Am} = \left[\frac{D^o_{AC}}{D_{AB}}\left(y_B - \frac{b}{a}y_A\right) + \frac{D^o_{AC}}{D_{AC}}\left(y_c + \frac{c}{a}y_A\right) + \frac{D^o_{AC}}{D_{k,A}}\right]^{-1} \tag{11}$$

$$D^*_{Bm} = \left[\frac{D^o_{AC}}{D_{AB}}\left(y_A - \frac{a}{b}y_B\right) + \frac{D^o_{AC}}{D_{BC}}\left(y_c + \frac{c}{b}y_B\right) + \frac{D^o_{AC}}{D_{k,B}}\right]^{-1} \tag{12}$$

in which we have used the ideal gas law to write $C_T = C^o_T/\theta$. Further, we assume that the molecular diffusion coefficients are proportional to $T^{1.75}$, while the Knudsen diffusivities vary as $rT^{0.5}$, giving

$$D^*_{Am} = \left[\frac{d_{AB}}{\theta^{1.75}}\left(y_B - \frac{b}{a}y_A\right) + \frac{1}{\theta^{1.75}}\left(y_C + \frac{c}{a}y_A\right) + \frac{d_{Ak}}{\rho\theta^{0.5}}\right]^{-1} \tag{13}$$

$$D^*_{Bm} = \left[\frac{d_{AB}}{\theta^{1.75}}\left(y_A - \frac{a}{b}y_B\right) + \frac{d_{BC}}{\theta^{1.75}}\left(y_C + \frac{c}{b}y_B\right) + \frac{d_{Bk}}{\rho\theta^{0.5}}\right]^{-1} \tag{14}$$

To complete the mass transfer model, it is necessary to specify the reaction kinetics and the pore volume distribution $f(r)$. For

the former, we consider a general nonlinear kinetic expression of the form

$$\hat{R}_A(C_A, C_B, T) = k_o C_A^n C_B^m e^{-E_R/R_g T} \tag{15}$$

which, under the assumption of the ideal gas law, yields

$$\hat{R}_A^* = \frac{y_A^n y_B^m e^{-\nu(1-\theta)/\theta}}{(y_A^o)^n (y_B^o)^m \theta^{(n+m)}} \tag{16}$$

In all the computations reported here, m was taken to be unity, while n was chosen as one or two. For the pore volume distribution, we assume log-normal forms for the macropore and micropore contributions:

$$\frac{d\epsilon_m}{dr} = \sqrt{\frac{1}{2\pi}} \frac{\epsilon_m}{r\sigma_m} \exp\left[-(\ln r/\mu_m)^2/2\sigma_m^2\right] \tag{17}$$

$$\frac{d\epsilon_i}{dr} = \sqrt{\frac{1}{2\pi}} \frac{\epsilon_i}{r\sigma_i} \exp\left[-(\ln r/\mu_i)^2/2\sigma_i^2\right] \tag{18}$$

As mentioned earlier, the structure could comprise randomly interconnected macropores and micropores or nonoverlapping microporous grains. In either case, we may define the combined pore volume distribution

$$f(r) = \frac{d\epsilon_i}{dr} + \frac{d\epsilon_m}{dr} \tag{19}$$

for the estimation of effective pellet diffusivities as in Eqs. 9 and 10. For the case of the nonoverlapping microporous grain model, this entails the assumption that the tortuosity factors for macropore and micropore diffusion are equal. Equations 17–19 combine to yeld the dimensionless form

$$f(\rho)d\rho = \frac{1}{\rho}\sqrt{\frac{1}{2\pi}}\left[\frac{\epsilon_i}{\sigma_i}\exp\left[-(\ln\rho)^2/2\sigma_i^2\right] + \frac{\epsilon_m}{\sigma_m}\exp\left[-(\ln\rho/\mu_m^*)^2/2\sigma_m^2\right]\right]d\rho \tag{20}$$

Heat transfer

As in the prior work (Bhatia, 1988), it was assumed that heat transfer is controlled by boundary layer processes and internal temperature gradients are negligible. This is consistent with theory as well as experience (Froment and Bischoff, 1979) and yields the dimensionless energy balance

$$\theta - 1 = \frac{\psi D_{eA}^*(1)}{\theta}\left(\frac{dy_A}{d\eta}\right)_{\eta=1} \tag{21}$$

which is to be solved simultaneously in conjunction with the above mass transfer model to calculate the pellet temperature θ. To complete the model, it now remains to specify the thermodynamic relation satisfied by the critical pore size r_c (or its dimensionless counterpart ρ_c). This is the vapor-liquid equilibrium condition developed below.

Vapor-liquid equilibrium

At any position in the pellet pores larger than the critical size r_c will be vapor-filled, while those smaller than this size will be liquid-filled. The vapor-liquid equilibrium condition will be satisfied for pores of size r_c, yielding (Bhatia, 1988)

$$\frac{\hat{f}_i^v}{\hat{f}_i^l} = \exp\left(-2\sigma\cos\hat{\theta}\bar{v}_i/r_c R_g T\right) \tag{22}$$

which, upon assuming ideal mixtures for liquid and vapor and ideal gas pure component vapors, reduces to

$$\frac{y_i P}{x_i P_i^o} = \exp\left(-2\sigma\cos\hat{\theta}\bar{v}_i/r_c R_g T\right) \tag{23}$$

for the condensible components such as A and C (Bhatia, 1988). For the noncondensible components such as B, the derivation follows that of Henry's law (Smith and Van Ness, 1987) and the above assumptions transform Eq. 22 to

$$\frac{y_i P}{x_i H_i} = \exp\left(-2\sigma\cos\hat{\theta}\bar{v}_i/r_c R_g T\right) \tag{24}$$

where H_i is the Henry's law constant for noncondensible component i. Equations 23 and 24 combine to yield the dimensionless condition

$$\sum_i \frac{y_i}{p_i^{o*}} \exp\left[h_i\alpha(\theta)/\rho_c\theta\right] = 1 \tag{25}$$

which must be satisfied by the critical pore size ρ_c. Here P_i^{o*} equals P_i^o/P for the condensible components and H_i/P for the noncondensible components, $h_i = \bar{v}_i/\bar{v}_A$, and $\alpha(\theta) = 2\sigma\cos\hat{\theta}\bar{v}_A/\mu_i R_g T_o$. As in the prior work, α is considered to be a function of θ because of the dependency of surface tension σ on temperature. For the system under consideration, Eq. 25 reduces to

$$\frac{y_A}{P_A^{o*}(\theta)} e^{\alpha(\theta)/\rho_c\theta} + \frac{y_B}{P_B^{o*}(\theta)} e^{\alpha(\theta)h_B/\rho_c\theta} + \frac{y_C}{P_C^{o*}(\theta)} e^{\alpha(\theta)h_C/\rho_c\theta} = 1 \tag{26}$$

which must be solved in conjunction with Eqs. 6–10, 13, 14, 16, 20 and 21 to obtain the profiles of mole fraction and critical pore size ρ_c. Before this can be done, it is necessary to specify the functional forms of $\alpha(\theta)$, $P_A^{o*}(\theta)$, $P_B^{o*}(\theta)$ and $P_C^{o*}(\theta)$. For the former, we assume a linear dependence of surface tension on temperature over the narrow range of conditions to be encountered (Reid et al., 1977), resulting in

$$\alpha(\theta) = f + g\theta \tag{27}$$

where f and g are constants. For the dimensionless vapor pressures, P_A^{o*} and P_C^{o*} we assume the validity of the Clausius-Clapeyron relationship and set

$$P_A^{o*} = P_{Ao}^* \exp\left[-\Delta H_A^*(1-\theta)/\theta\right] \tag{28}$$

$$P_C^{o*} = P_{Co}^* \exp\left[-\Delta H_C^*(1-\theta)/\theta\right] \tag{29}$$

where $P_{Ao}^* = P_A^o(T_o)/P$ and $P_{Co}^* = P_C^o(T_o)/P$ are the dimension-

less vapor pressures at temperature T_o. For the dimensionless Henry's law constant P_B^{o*} also, we assume, following Denbigh (1981), a temperature dependence of the above form,

$$P_B^{o*} = P_{Bo}^{*} \exp\left[-\Delta H_B^{*}(1-\theta)/\theta\right] \tag{30}$$

in which ΔH_B^{*} is to be interpreted as the dimensionless heat of desorption of B from the ideal solution, and $P_{Bo}^{*} = H_B(T_o)/P$ is the dimensionless Henry's law constant for B at temperature T_o.

Results and Discussion

Numerical procedure

Equations 6–10, 13, 14, 16, 20, 21 and 26–30 form a coupled system of equations to be solved simultaneously to obtain the pellet temperature θ and the profiles of y_A, y_B and ρ_c. The orthogonal collocation technique (Finlayson, 1972) was used to convert the differential equations (Eqs. 6 and 7) to algebraic equations for the mole fractions at the collocation points, with the integrals in Eqs. 9 and 10 being evaluated by Gauss-Laguerre quadrature (Carnahan et al., 1969). This resulted in a system of nonlinear equations in the mole fractions which was solved in conjunction with Eq. 26 by the Newton-Raphson method. A suitable value of the pellet temperature θ was chosen, and the values of ρ_c and the mole fractions of A and B at the collocation points as well as the surface flux ($dy_A/d\eta$ at $\eta = 1$) were obtained from the solution of the above system. Equation 21 was then used to calculate the value of ψ consistent with the chosen pellet temperature. This procedure reduced the number of simultaneous nonlinear equations to be solved by one, since the alternative procedure is to choose the value of ψ and solve Eq. 21 simultaneously with the above system. A total of nine internal collocation points and 15 quadrature points were used and, upon varying their number, were found to yield sufficient accuracy.

As developed above, the model contains several parameters. All of these parameters, however, are physicochemical constants of the system and can be independently measured or estimated, so that there are no arbitrary "adjustable" constants. Table 1 lists the values of the parameters that were unchanged in most of the computations performed. The transport and thermodynamic parameters were chosen so that the properties of A, B and C corresponded with those of naphthalene, hydrogen, and cyclohexane, respectively, at 625 K, and are similar to those encountered in high-pressure hydrotreating. The other parameters, whose values varied in the computations, are σ_i, σ_m, y_A^o, ψ and ϕ. The bulk vapor was taken as comprising only A and B so that $y_B^o = 1 - y_A^o$. Since the Thiele modulus ϕ depends also on the external mole fractions y_A^o and y_B^o, it was relaced by the independent parameter ϕ_T which is defined as

$$\phi_T = R_o\left[\frac{\tau S_o k_o C_T^{o(n+m-1)}\, e^{-E_R/R_gT}}{\epsilon D_{AC}^{o}}\right]^{1/2} \tag{31}$$

and which is related to ϕ by

$$\phi = \phi_T (y_A^o)^{(n-1)/2} (y_B^o)^{m/2} \tag{32}$$

Table 1. Parameter Values Used in Computations

Parameter	Value	Parameter	Value
ν	25	μ_m^{*}	10
m	1	d_{AB}	0.08
n	1	d_{BC}	0.072
a	1	d_{Ak}	0.194
b	5	d_{Bk}	0.024
c	2	ΔH_A^{*}	8.272
f	3.455	ΔH_B^{*}	0.1728
g	−3.175	ΔH_C^{*}	5.728
h_B	0.167	P_{A0}^{*}	0.2
h_C	0.667	P_{B0}^{*}	17.0
ϵ_i	0.5	P_{C0}^{*}	1.5
ϵ_m	0.1		

Numerical results

From the solution obtained using the above numerical procedure, the pellet effectiveness factor, which as usual is the ratio of the actual reaction rate to that obtained in the absence of thermal and diffusional resistances, was calculated by

$$E = \frac{3(\theta - 1)}{\psi\phi^2 y_A^o} \tag{33}$$

In all the computations reported here, the bulk vapor comprises only A and B, as mentioned earlier. Figure 1 shows the variation of the effectiveness factor with Thiele modulus ϕ_T for various values of ψ. Although only two steady states are shown, it is clear that a third, high-reactivity, steady-state branch must also exist. That branch, corresponding to extremely high effectiveness factors (even larger than 1,000) is not shown because the corresponding temperatures are impractically high. Since the middle steady state is always unstable, it is only the lowest branch that is feasible in practice. Hence, all further computations reported are for the lowest effectiveness factor branch. The curves of Figure 1 are typical also of single-phase reaction, except for low values of ϕ_T or for low values of ψ at a given ϕ_T. For such situations, we see that the effectiveness factor drops

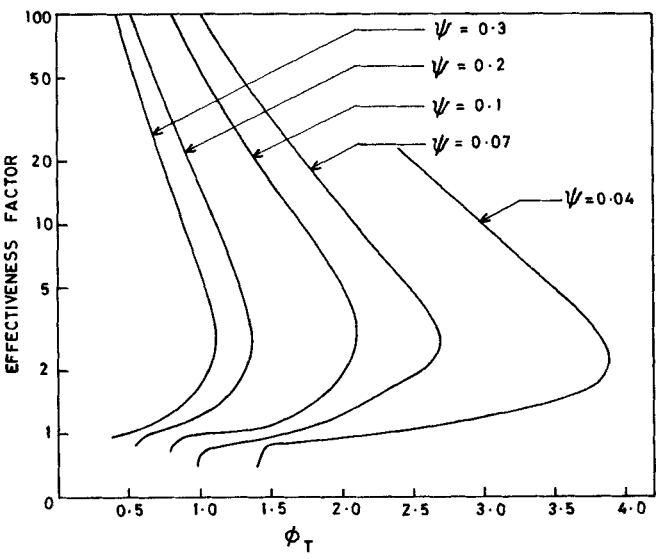

Figure 1. Effectiveness factor vs. Thiele modulus for various values of ψ and $\sigma_i = \sigma_m = 0.2$, $y_A^o = 0.1905$.

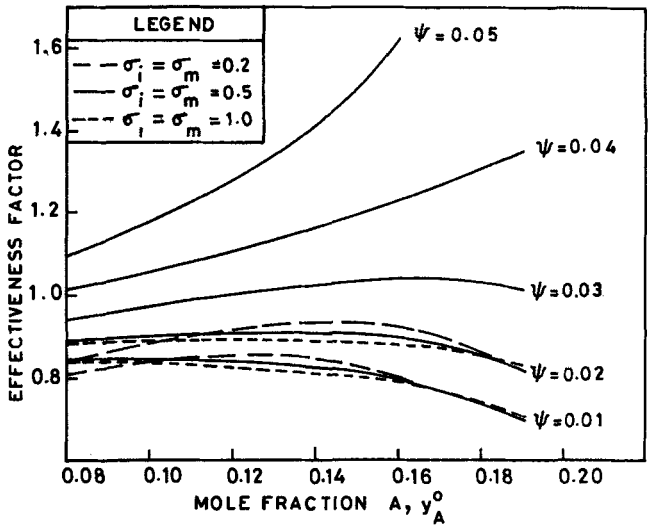

Figure 2. Effectiveness factor vs. mole fraction *A* in bulk vapor for values of ψ and $\phi_T = 3.5$.

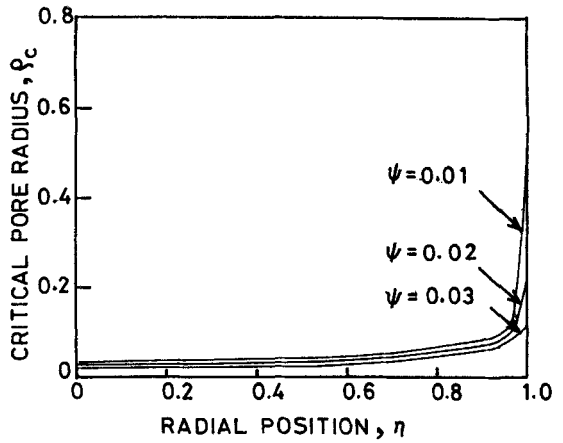

Figure 3. Profiles of critical pore radius ρ_c, below which liquid filling occurs for values of ψ and $\phi_T = 3.5$, $\sigma_i = \sigma_m = 0.2$, $y_A^o = 0.1905$.

precipitously and, as will be subsequently shown, this is due to greatly increased capillary condensation and filling of the pores with liquid.

The solid curves in Figure 2 depict the effect of y_A^o, the bulk mole fraction of A, and ψ on the effectiveness factor for the parameter values of Table 1 and $\phi_T = 3.5$, $\sigma_i = \sigma_m = 0.5$. At the larger values of ψ such as 0.04 and 0.05, the effectiveness factor increases continuously with increase in mole fraction y_A^o of the condensible component even up to the saturation value of 0.1905. At this value of y_A^o, the external vapor is easily confirmed to be saturated for the values of P_{Ao}^* and P_{Bo}^* in Table 1. This increase in the effectiveness factor with increase in y_A^o is consistent with the normal behavior expected for noncondensing systems, since the bulk vapor is component B predominantly. At the lower values of ψ the effectiveness factor, however, shows a maximum with increase in y_A^o before reducing as the saturation value is approached. This anomalous behavior is easily seen to be caused by capillary condensation effects, since, at the lower values of ψ, the relative rate of heat generation is small resulting in lower values of pellet temperature and consequently in increased condensation. The increased capillary condensation in turn reduces the pore space available for vapor-phase transport and results in lower effectiveness factor. This reasoning is justified by Figure 3 which shows the profile of the critical pore radius ρ_c, below which liquid filling occurs, at various values of ψ and $\phi_T = 3.5$, $\sigma_i = \sigma_m = 0.2$, $y_A^o = 0.1905$. As expected at the lower values of ψ, the critical pore radius is larger resulting in lower effectiveness factor. With reduction in ψ, ρ_c increases most near the outer surface, so that the mass transfer resistance increases more in this region, reducing the penetration of the reactants and consequently the effectiveness factor.

Also superimposed on Figure 2 are the curves of effectiveness factor vs. y_A^o *for* $\sigma_i = \sigma_m = 0.2$ and 1.0, and $\psi = 0.01$, 0.02. The behavior is similar to that seen for $\sigma_i = \sigma_m = 0.5$, with changes in the values of the standard deviation having only a small effect. However, at the lower values of y_A^o, there appears to be an optimum value of the standard deviation, since the effectiveness factor is the largest for $\sigma_i = \sigma_m = 0.5$. Over most of the range, however, effectiveness factor is largest for $\sigma_i = \sigma_m = 0.2$, but near the saturation value of y_A^o the effectiveness factor is lowest for $\sigma_i = \sigma_m = 0.2$.

Figure 4 illustrates the variation of effectiveness factor with y_A^o at various values of ψ, for $\phi_T = 0.7$ and $\sigma_i = \sigma_m = 0.2$, with the rest of the parameters as in Table 1. The behavior is much more interesting for the lower value of ϕ_T and shows considerable differences as compared to the curves for $\phi_T = 3.5$ as shown in Figure 2. At the lower value of ϕ_T, the effectiveness factor vs. y_A^o curve shows a maximum even at the high values of ψ of 0.4. As discussed above, this maximum is due to capillary condensation effects which are even stronger at the lower value of ϕ_T, since higher mole fractions of the condensible A are now possible in the pellet. However, with reduction in ψ, the effectiveness factor goes through a minimum before rising again as seen by the curves for $\psi = 0.30$ and 0.20.

When the value of ψ is further reduced to 0.10, even more

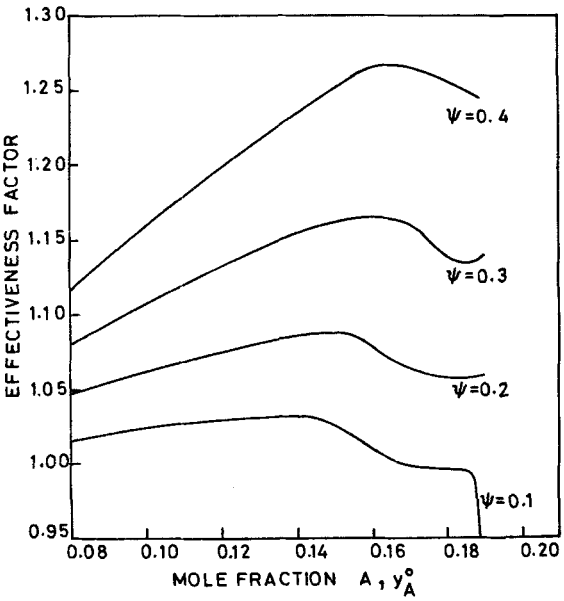

Figure 4. Effectiveness factor vs. mole fraction *A* in the bulk vapor for values of ψ and $\phi_T = 0.7$, $\sigma_i = \sigma_m = 0.2$.

interesting behavior is found with the effectiveness factor dropping precipitously as the saturation value of $y_A^o = 0.1905$ is approached. The minimum in the value of effectiveness with increase in y_A^o is due to the fact that the temperature and hence reaction rate also increase with increase in y_A^o for $\psi = 0.2$ and above, as shown in Figure 5. If this increase in rate is sufficient, it may more than compensate for the effect of enhanced capillary condensation with increase in y_A^o, resulting in increase in effectiveness. Hence, the value of effectiveness has a minimum. At sufficiently low values of ψ such as 0.10, however, the thermal effect is much weaker and capillary condensation reduces the transport. Therefore, reaction rate and temperature and effectiveness factor also are reduced precipitously, as the saturation value of y_A^o is approached. This is also reflected in the curve for $\psi = 0.10$ in Figure 5.

Further support for this argument is also available in Figure 6 which depicts the profiles of critical pore radius ρ_c for various values of ψ and $\phi_T = 0.7$, $\sigma_i = \sigma_m = 0.2$, $y_A^o = 0.1905$. Starting from $\psi = 0.4$ with decrease in ψ down to 0.2, the critical pore radius is higher for all η indicating increased liquid filling throughout the particle. With a further decrease in ψ to 0.11, the critical pore radius near the surface increases by a very large magnitude causing a large mass transfer resistance near the particle surface, thus severely restricting penetration of reactants and accounting for the large drop in effectiveness and temperature.

An interesting feature of the curve of $\psi = 0.11$ in Figure 6 is that the critical pore radius within most of the particle interior is actually less than that of $\psi = 0.2$ and the larger values of ψ, but this is explained by the reduced penetration of the condensible reactant A. This is borne out by the mole fraction profiles shown in Figure 7 indicating the sharp drop in mole fraction of A within the pellet interior for $\psi = 0.11$. For $\psi = 0.2$, the mole fraction A near the surface is larger than that for $\psi = 0.4$, because of lower temperature and hence lower mass transfer resistance. However, this increases the value of ρ_c and mass

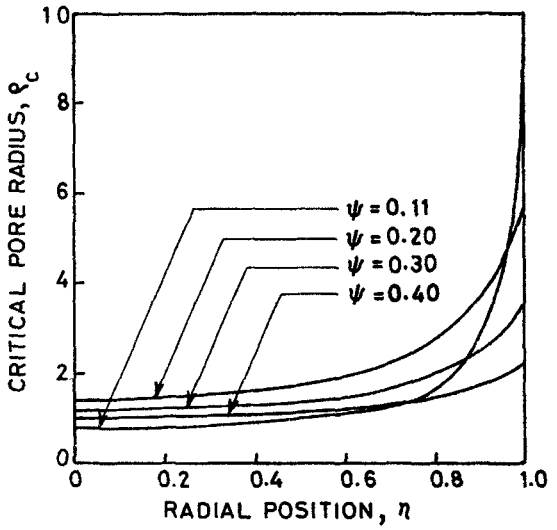

Figure 6. Profiles of critical pore radius ρ_c, below which liquid filling occurs for values of ψ and $\phi_T = 0.7$, $\sigma_i = \sigma_m = 0.2$, $y_A^o = 0.1905$.

transfer resistance inside so that at some point in the pellet interior the two profiles intersect.

Figure 8 shows the mole fraction profiles for various values of y_A^o for $\phi_T = 0.7$, $\psi = 0.10$ and $\sigma_i = \sigma_m = 0.2$. Consistent with the above arguments and Figure 4, the mole fraction A in the pellect interior increases with increase in y_A^o up to 0.18. Due to computational difficulty, the curve for $y_A^o = 0.1905$ could not be obtained. However, it may be expected to show a large decrease compared to the other curves consistent with the sharp drop in effectiveness factor expected from Figure 4.

Figure 9 shows the effectivenss factor vs. y_A^o curves for the case of a reaction which is second order with respect to the condensible reactant A. The results are qualitatively similar to the case for $n = 1$, but the maximum in the effectiveness factor is

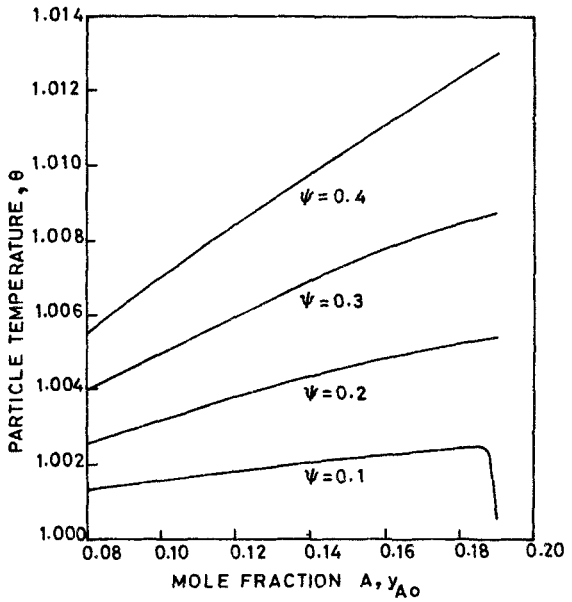

Figure 5. Particle temperature θ vs. bulk mole fraction y_A^o at values of ψ for $\phi_T = 0.7$ and $\sigma_i = \sigma_m = 0.2$.

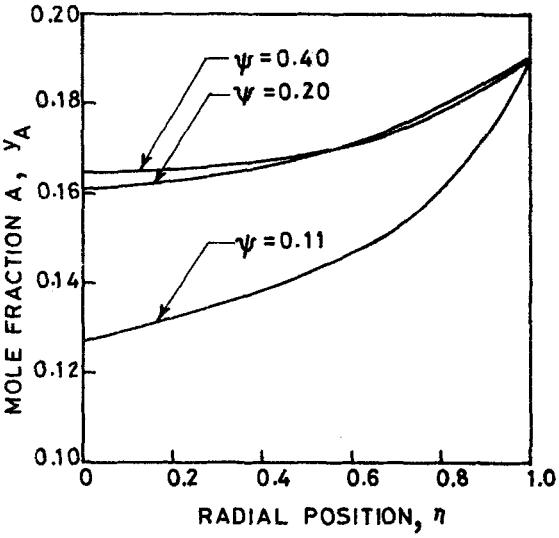

Figure 7. Profiles of mole fraction y_A at values of ψ, for $\phi_T = 0.7$, $y_A^o = 0.1905$ and $\sigma_i = \sigma_m = 0.2$.

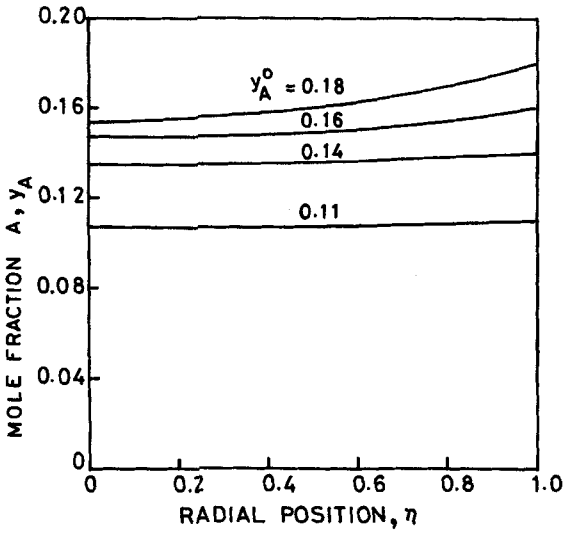

Figure 8. Profiles of mole fraction y_A at values of y_A^o for $\phi_T = 0.7$, $\psi = 0.10$, $\sigma_l = \sigma_m = 0.2$.

much more pronounced, and for the lower values of ψ of 0.05 and 0.10 the subsequent drop is also relatively large.

It is clear from the above discussion that a variety of interesting behavior occurs in catalyst pellets because of the interplay of capillary condensation phenomena with thermal and mass transfer effects. Such effects have previously not been explored, and this and the prior work (Bhatia, 1988) have developed the necessary tools for the study of these problems. While this paper considers the effect of standard deviation in pore-size distribution and multicomponent diffusion, the prior work considered uniformly-sized micropores and macropores with no bulk motion. Because of the complexity introduced by the multicomponent case and the numerical difficulty associated with setting σ_m and σ_l very small in Eqs. 17 and 18, the results of the two papers were not compared.

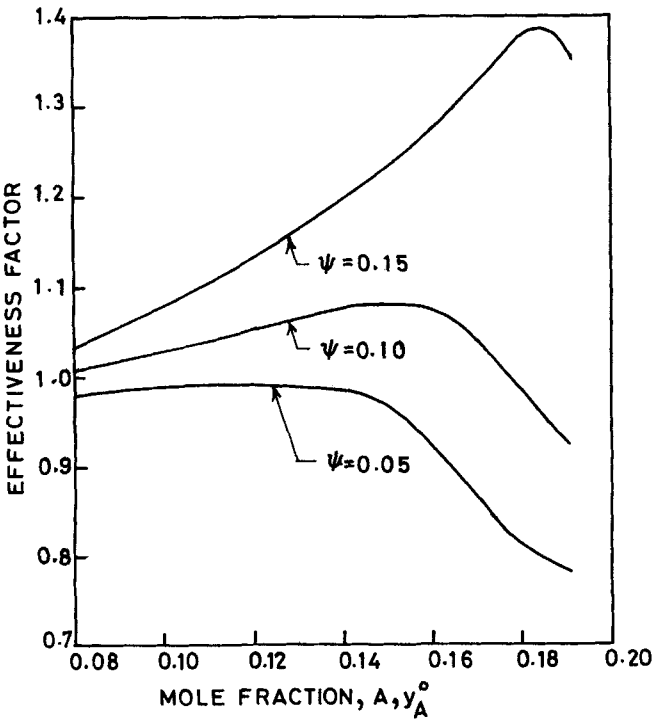

Figure 9. Effectiveness factor vs. bulk mole fraction of *A* for values of ψ and $\phi_T = 3.5$, $\sigma_l = \sigma_m = 0.2$, $n = 2$, $m = 1$.

Other parameters are the same as in Table 1.

It is noteworthy that the anomalous behavior of the effectiveness factor in Figure 4 is qualitatively similar to that seen in the Figures of Kim and Kim (1981a), although a more direct comparison cannot be made since the kinetic and diffusional parameters in their experimental system are not all known. Further, multiplicity of the partial wetting effectiveness factors with more than three steady states may also exist for other parameter values. Because of the large number of parameters, the effort required to investigate and identify regions of multiplicity would be extensive and this aspect was therefore not studied here. For a particular experimental system with known parameter values, however, the existence of multiplicities such as those found by Kim and Kim (1981a) could be investigated and confirmed.

Another feature to note is that in spite of capillary condensation a significant portion of the pore space is vapor-filled. Figure 3 shows ρ_c to lie in the range of 0.2 to 0.5 over much of the pellet interior, and as high as 7 at the pellet surface for the parameter values chosen for the computations in that figure. Since the dimensionless mean micorpore radius is unity and the dimensionless mean macropore size chosen is 10, as seen in Table 1, over most of the pellet interior the majority of the pore space is vapor-filled. At the surface, however, the micropores are mostly liquid-filled, and even a significant portion of the macropores are liquid-filled. For the parameter values used for the computations in Figure 6, over the majority of the particle, ρ_c is in the range of 1 to 2 so that considerable capillary condensation occurs in the micropores, but a significant portion of the micropores is also vapor-filled. Near the surface, ρ_c is higher, even as large as 10, so that some condensation occurs even in the macropores but a large portion of the macropores are still vapor-filled. These results contradict the prior studies of partial wetting mentioned earlier, which have assumed complete internal wetting of catalyst pellets. The current model, based on a proper representation of the capillary condensation equilibria and the related thermodynamics, would appear to be more realistic and establishes the framework for the analysis of such problems. While we considered the case of particles exposed to vapor, other situations such as that of fully or partially externally-wetted particles could also be considered by the present approach to study the various possibilities that can arise in trickle-bed reactors.

Under conditions with almost complete capillary condensation and liquid filling of the pores, the present model, which neglected radial liquid phase transport, would predict zero effectiveness. Hence, it is not possible to compare with the existing models which consider complete internal wetting and therefore only liquid-phase transport. It is easily estimated, however, that, since vapor-phase diffusivities are about 10^4 times larger than the liquid-phase values, for liquid-phase transport to be significant at the high pressures corresponding to hydroprocessing (100–200 atm) the pore volume occupied by liquid must be at least hundred times that occupied by vapor. As shown in this work, this cannot be actually achieved, since a significant portion of the pore space is always vapor-filled in practice because of exothermicity.

Acknowledgment

The author thanks Mr. D. N. Jaguste for computational assistance in preparing Figure 1.

Notation

a, b, c = stoichiometric factors
C_A^o, C_B^o = bulk concentrations of A and B
C_T = total gas-phase concentration
C_T^o = C_T at bulk conditions
$d_{AB} = D_{AC}^o/D_{AB}^o$
$d_{BC} = D_{AC}^o/D_{BC}^o$
$d_{Ak} = D_{AC}^o/D_{k,A}(\mu_i)$
$d_{Bk} = D_{AC}^o/D_{k,B}(\mu_i)$
D_{ij} = binary diffusivity
D_{ij}^o = D_{ij} at bulk temperature
D_{im} = Eq. 5
$D_{Am}^* = D_{Am}/D_{AC}^o$
$D_{Bm}^* = D_{Bm}/D_{AC}^o$
D_{eA}^* = Eq. 9
D_{eB}^* = Eq. 10
$D_{k,i}$ = Knudsen diffusivity for component i
E = effectiveness factor
E_R = activation energy
f = Eq. 27
$\hat{f}_i^{\ell}$ = mixture fugacity of component i in liquid phase
$\hat{f}_i^{v}$ = mixture fugacity of component i in vapor phase
$f(r)$ = pore-size distribution
g = Eq. 27
h = external heat transfer coefficient
$h_i = \bar{v}_i/\bar{v}A$
H_i = Henry's law constant
$\Delta H_A^* = \Delta H_A R_g T_o$, dimensionless enthalpy of vaporization of pure A
$\Delta H_B^* = \Delta H_B/R_g T_o$, dimensionless enthalpy of desorption
$\Delta H_C = \Delta H_C R_g T_o$, dimensionless enthalpy of vaporization
k_o = constant, Eq. 15
m, n = order
$N_i(r)$ = flux of component i in pore of radius r
N_i = flux of component i in pellet
P = pressure
P_i^o = vapor pressure for condensible components and Henry's law constant for noncondensible components at temperature T
$P_i^{o*} = P_i^o/P$
$P_{io}^* = P_i^o(T_o)/P$
r = pore radius
r_c = critical pore radius
R = radial position
R_o = pellet radius
R_g = universal gas constant
$\hat{R}_i$ = reaction rate for component i
$\hat{R}_A^* = \hat{R}_A(C_A, C_B, T)/\hat{R}_A(C_A^o, C_B^o, T_o)$
S_o = pellet internal surface area
T = temperature
T_o = bulk temperature
$\bar{v}_i$ = partial molar volume of component i
y_i = mole fraction of component i
y_i^o = bulk mole fraction of component i

Greek letters

$\alpha(\theta) = 2\sigma \cos\hat{\theta}\,\bar{v}_A/\mu_i R_g T_o$
ϵ = total porosity
ϵ_i = microporosity
ϵ_m = macroporosity
$\eta = R/R_o$
μ_i = mean micropore radius
μ_m = mean macropore radius
$\mu_m^* = \mu_m/\mu_i$
$\nu = E_R/R_g T_o$
$\phi = R_o\sqrt{\tau S_o \hat{R}_A(C_A^o, C_B^o, T_o)/\epsilon D_{AC}^o C_A^o}$
ϕ_T = Eq. 31
$\psi = -\Delta H_R D_{AC}^o C_T^o \epsilon/\tau R_o h T_o$
$\rho = r/\mu_i$
$\rho_c = r_c/\mu_i$
σ = surface tension
σ_i = standard deviation in micropore-size distribution
σ_m = standard deviation in macropore-size distribution
τ = tortuosity factor
$\theta = T/T_o$
$\hat{\theta}$ = contact angle

Literature Cited

Bhatia, S. K., "Steady-State Multiplicity and Partial Internal Wetting of Catalyst Particles," *AIChE J.*, **34,** 969 (1988).
Carnahan, B. C., H. A. Luther, and J. O. Wilkes, *Applied Numerical Methods,* Wiley, New York (1969).
Denbigh, K., *Principles of Chemical Equilibrium,* Cambridge University Press, Cambridge (1981).
Drobyshevich, V. I., V. A. Kirillov, and N. A. Kuzin, "A Mathematical Model of the Process with Phase Transition on the Porous Catalyst Pellet," *Chem. Eng. Commun.*, **22,** 151 (1983).
Feng, C., and W. E. Stewart, "Practical Models for Isothermal Diffusion and Flow of Gases in Porous Solids," *Ind. Eng. Chem. Fund.*, **12,** 143 (1973).
Finlayson, B., *The Method of Weighted Residuals and Variational Principles,* Academic Press, New York (1972).
Froment, G. F., and K. B. Bischoff, *Chemical Reactor Analysis and Design,* Wiley, New York (1979).
Hanika, J., K. Sporka, V. Ruzicka, and J. Hrstka, "Measurement of Axial Temperature Profiles in an Adiabatic Trickle-Bed Reactor," *Chem. Eng. J.*, **12,** 193 (1976).
Harold, M. P., "Partially Wetted Catalyst Performance in the Consecutive-Parallel Network," *AIChE J.*, **34,** 980 (1988).
Herskowitz, M., "Wetting Efficiency in Trickle-Bed Reactors. The Overall Effectiveness Factor of Partially Wetted Catalyst Particles," *Chem. Eng. Sci.*, **36,** 1665 (1981a).
———, "Wetting Efficiency in Trickle-Bed Reactors: Its Effect on Reactor Performance, "*Chem. Eng. J.*, **22,** 167 (1981b).
Hite, R. H., and R. Jackson, "Pressure Gradients in Catalyst Pellets in the Intermediate Diffusion Regime," *Chem. Eng. Sci.*, **32,** 703 (1977).
Hu, R., and T. C. Ho, "Steady State Multiplicity in an Incompletely Wetted Catalyst Particle," *Chem. Eng. Sci.*, **42,** 1239 (1987).
Jackson, R., *Transport in Porous Catalysts,* Elsevier, Amsterdam (1977).
Kehoe, J. P. G., and R. Aris, "Communications on the Theory of Diffusion and Reaction: IX. Internal Pressure and Forced Flow for Reactions with Volume Change," *Chem. Eng. Sci.*, **28,** 2094 (1973).
Kim. D. Y., and Y. G. Kim, "An Experimental Study of Multiple Steady States in a Porous Catalyst Due to Phase Transition," *J. Chem. Eng. Japan,* **14,** 311 (1981a).
———, "Simulation of Multiple Steady States in a Porous Catalyst Due to Phase Transition," *J. Chem. Eng. Japan,* **14,** 318 (1981b).
Leung, K., and H. W. Haynes, Jr., "Diffusion and Reaction in Bidisperse Structured Catalyst Particles," *Chem. Eng. Sci.*, **39,** 1815 (1984).
Mills, P. L., and M. P. Dudokovic, "Application of the Method of Weighted Residuals to Mixed Boundary Value Problems: Dual-Series Relations," *Chem. Eng. Sci.*, **35,** 1557 (1980)
———, "Integral Equation Solution for the Effectiveness Factor of Partially Wetted Catalysts," *Ind. Eng. Chem. Fund.*, **21,** 90 (1982).
Ramachandran, P. A., and J. M. Smith, "Effectiveness Factors in Trickle-Bed Reactors," *AIChE J.*, **25,** 538 (1979).
Reid, R. C., J. M. Prausnitz, and T. K. Sherwood, *The Properties of Gases and Liquids,* McGraw-Hill, New York (1977).
Sakornwimon, W., and N. D. Sylvester, "Effectiveness Factors for Partially Wetted Catalysts in Trickle-Bed Reactors," *Ind. Eng. Chem. Process Des. Dev.*, **21,** 16 (1982).
Satterfield, C. N., and F. Ozel, "Direct Solid-Catalyzed Reaction of a Vapor in an Apparently Completed Wetted Trickle-Bed Reactor," *AIChE J.*, **19,** 1259 (1973).
Satterfield, C. N., and P. F. Way, "The Role of the Liquid Phase in the Performance of a Trickle Bed Reactor," *AIChE J.*, **18,** 305 (1972).

Sedriks, W., and C. N. Kenney, "Partial Wetting in Trickle-Bed Reactors—The Reduction of Crotonaldehyde over a Palladium Catalyst," *Chem. Eng. Sci.*, **28,** 559 (1973).

Smith, C. M., and C. N. Satterfield," Some Effects of Vapor-Liquid Flow Ratio on Performance of a Trickle-Bed Reactor," *Chem. Eng. Sci.*, **41,** 839 (1986).

Smith, J. M., and H. C. Van Ness, *Introduction to Chemical Engineering Thermodynamics,* McGraw Hill, New York (1987).

Tan, C. S., "Effectiveness Factors of n-th Order Reactions for Incomplete Wetting of Particles in Trickle-Bed Reactors," *Chem. Eng. Sci.*, **43,** 1281 (1988).

Yentekakis, J. V., and C. G. Vayenas, "Effectiveness Factors For Reactions Between Volatile and Nonvolatile Components in Partially Wetted Catalysts," *Chem. Eng. Sci.*, **42,** 1323 (1987).

Manuscript received Nov. 2, 1988, and revision received May 3, 1989.